Impact of an exceptional winter flood on benthic oxygen and nutrient fluxes in a temperate macrotidal estuary: Potential consequences on summer deoxygenation

Vivien Hulot[1]*, Edouard Metzger[1]*,
Aubin Thibault de Chanvalon[2], Aurelia Mouret[1], Sabine Schmidt[3],
Bruno Deflandre[3], Sylvain Rigaud[4], Eric Beneteau[1],
Nicolas Savoye[3], Philippe Souchu[5], Yoann Le Merrer[5]
and Grégoire M. Maillet[1]

[1]UMR 6112 LPG, Université d'Angers, Université de Nantes, Université du Mans, CNRS, Angers, France,
[2]Université de Pau et des Pays de l'Adour, E2S UPPA, CNRS, IPREM, Pau, France, [3]Université de
Bordeaux, CNRS, Bordeaux INP, UMR5805 EPOC, Pessac, France, [4]Univ. Nîmes, UPR 7352 CHROME,
Nîmes, France, [5]IFREMER – LER, MPL, Nantes, France

Despite 20 years of control on eutrophication, episodes of summer hypoxia still occur in the Loire estuary, impacting water quality and posing a key scientific and management challenge. This work aimed to quantify the contribution of the benthic compartment to hypoxia in the Loire estuary by direct measurement of water−sediment fluxes and an in-depth understanding of the seasonal variations of oxides and phosphorus stocks. During the summer's low-discharge period, results show that the iron oxide-rich deposit is stable under hypoxic conditions, limiting the release of dissolved phosphorus into the overlying water column. The high nitrate content of the water column appears to be an important oxidizer of iron during hypoxic periods, limiting dissolved phosphorus leakage and aggravation of hypoxia. During the exceptional winter flood, significant sediment erosion associated with bubbling phenomena (attributed to methane efflux) created severe fractures in the sediment and stimulated water−sediment exchange. During the following months, these fractures were progressively filled, which decreased the intensity of benthic fluxes. However, due to the high residence time in the water during the summer period, a simple model demonstrated that benthic contributions were sufficient to directly (by direct oxygen consumption) or indirectly (by promoting ammonia oxidation) affect the oxygen stock in the water column during the low-discharge period. Our study demonstrates the importance of the benthic compartment in the occurrence of hypoxia and the obvious lack of knowledge to illustrate and model the biogeochemical functioning of the estuary.

KEYWORDS

estuary, water sediment exchanges, hypoxia, oxides-phosphorus interactions, flood

1 Introduction

Estuarine systems are key areas for the life cycle of many organisms, such as European eel *Anguilla anguilla* (Steinbach, 2001; Blanchet-Letrouvé et al., 2013) as well as for the implementation of human activity (Nichols et al., 1986). In terms of surface area, the Loire macrotidal system is the second most important estuary of the French metropolitan coastline. The intensity of human implementation is illustrated by the presence of the Nantes metropolis (665,000 inhabitants) and the intense harbor activities (covering 2,700 ha and hosting more than 2,000 ferries annually).

The water residence time in the Loire ranges from 3 to 30 days, mainly controlled by the Loire River discharge and modulated by tidal forces (Guillaud et al., 2008). The Loire discharge variability is a keystone parameter when trying to understand its water column properties. Firstly, the water residence time drives the duration of interaction time between sediment, water, and atmosphere within the estuary. Secondly, the fluvial discharge intensity controls the deposition of particles and, thus, the organic matter input on the water body's bed, known as the critical factor of benthic fluxes intensity (Burdige, 2006). Finally, tidal forces and water-discharge intensity modulate current velocity, activating possible advection processes in permeable sediment, inducing, in turn, the enhancement of benthic exchanges (Janssen et al., 2005).

During flood events, the Loire River discharge can reach up to 7,000 $m^3 \ s^{-1}$, repeatedly causing significant damages to floodplains and anthropic infrastructures (De Blois and Wind, 1995). In addition, the shear stress induced by high-velocity currents during floods (i.e., riverine discharge > 4000 $m^3 \ s^{-1}$, Sanchez and Levacher, 2008) may resuspend fairly cohesive sediments, generating the release of reduced compounds and associated nutrients that may affect the general biogeochemical functioning of the estuary and its adjacent coastal environment. Such important reworking of the sediment makes flood the key factor for trace metal distribution throughout the estuarine system and ultimately towards the ocean (Cheviet et al., 2002; Dhivert et al., 2015; Coynel et al., 2016). During low-discharge periods (down to few $m^3 \ s^{-1}$), increased water residence time favors seasonal deoxygenation with oxygen concentrations of below 2–3 mg L^{-1} (Ratmaya et al., 2019). Estuarine hypoxic events are highly variable in space and time due to a combination of physical and biological factors (Lanoux et al., 2013; Schmidt et al., 2019). Most of the oxygen consumption is attributed to aerobic and anaerobic respiration in the water column and sediment compartment (Center, 2005; Dai et al., 2008).

In macrotidal hyperturbid estuaries, hypoxia is often associated with the presence of turbidity maximum zones (TMZs) (Marchand, 1993; Talke et al., 2009; Lanoux et al., 2013; Lajaunie-Salla et al., 2017; Hayami et al., 2019), which are induced by tidal pumping due to tidal asymmetry (in which the flood phase is shorter, but with more intense current than the ebb phase; Jalón-Rojas et al., 2016). During periods of low fluvial discharge, usually in summer, TMZ is usually located upstream and causes high suspended particulate matter (SPM) concentrations of several hundred milligrams per liter. Such high SPM concentrations limit gas exchange and primary production and promotes pelagic microbial respiration (Abril et al., 2009). In addition, summer temperatures lower dissolved oxygen (DO), as DO solubility decreases while oxygen demand increases with increasing temperature.

Therefore, simplified scenarios often considered only river flow, temperature, and urban development to predict hypoxia risk in estuarine systems in the context of global and local changes (Lajaunie-Salla et al, 2018). Consequently, to limit hypoxia events, policy management offices focused on urban waste water treatments regulation and nutrient limitation (especially phosphorus) to control algae proliferation and thus organic matter (OM) availability. This strategy reduced hypoxia frequency in numerous estuarine systems, e.g., in the Providence River estuary (Oviatt et al., 2017), in Long Island Sound (Whitney and Vlahos, 2021) or the Pearl River Estuary (Yu and Gan, 2021). However, in the case of the Loire estuary, despite 20 years of nutrient input limitation (Ratmaya et al., 2019), summer hypoxia episodes still occur (Schmidt et al., 2019), impacting water quality and presenting a critical scientific and management challenge to be addressed.

In addition to the water column, the benthic compartment may play an underestimated role in the triggering and development of hypoxia (Center, 2005; Sohma et al., 2008; Lenstra et al., 2021). Especially in shallow systems, the sedimentary compartment can be the site of a significant fraction of OM remineralization (Burdige and Zheng, 1998; Huang et al., 2022). As a result, several hypoxia models include the contribution of the benthic compartment in shallow estuarine systems (Sohma et al., 2008) to explain the oxygen depletion of the water column.

By analogy with other estuarine systems, the Loire sediment compartment is likely to respond to local hypoxia through two complementary processes. Firstly, the direct DO consumption by OM degradation within the sediment enhances oxygen demand (Zhang et al., 2017). Secondly, the dissolution of iron and manganese oxides releases sedimentary inorganic phosphorus in the water column, favoring eutrophication (Canfield, 1989; Burdige, 1993; Anschutz et al., 1998). High concentration of iron oxides in the Loire estuarine sediment could efficiently prevent dissolved phosphorus to diffuse out of the sediment (Thibault de Chanvalon et al., 2016). However, when sediments are exposed to bottom water hypoxia, the enhanced dissolution of iron and manganese oxides may trigger a phosphorus flux to the water column. This input can act as a fertilizer that increases autochthonous primary production and thus subsequent aerobic MO degradation, consequently reinforcing hypoxia (Ghaisas et al., 2019). The impact of hypoxic exposure on benthic phosphorus mobility could be important as estuarine sediments are able to store a fraction of the phosphorus inherited from agricultural practices of the last 50 to 70 years. Therefore, assessing the seasonal role of benthic phosphorus remobilization is crucial for hypoxia management and should be explored by examining the balance between phosphorus sedimentation and binding capacity (Hupfer and Lewandowski, 2008; Carey and Rydin, 2011; Rydin et al., 2011).

To examine the potential contribution of the benthic compartment to hypoxia in the Loire estuary, this work aimed to quantify water–sediment fluxes and the evolution of oxides and phosphorus stocks in reactive sedimentary pools as a function of the season. The detailed objectives were as follows:

- Understand the factors controlling benthic oxygen and nutrient fluxes in an area subject to hypoxia;
- Examine the impact of an exceptional winter flood event on oxygen and nutrients benthic transfers;
- Estimate the relative contribution of sediment and water column to the total oxygen demand and nutrient budget throughout the hydrological year.

2 Methods

2.1 Study area and hydrological context

The watershed of the Loire River covers one-fifth of the surface area of metropolitan France. Its estuary flows from Ancenis reaching the Bay of Biscay (Nort-East Atlantic) at Saint-Nazaire. The most studied part of the estuary is located between Nantes and Saint-Nazaire, which represents the internal estuarine system and the area with the largest surface of immerged sediment. This zone covers nearly 220 km^2 and is composed of muddy sediments for 62% of its surface (Coynel et al., 2016). According to Hydroportail (Hydro, 2021), the mean Loire River discharge for the period 2020–2021 reaches 680 m^3 s^{-1}. Suspected to be the most reactive sediment to oxygen, this study focuses on muddy sediments from one of the sites in the estuary most exposed to hypoxic events. The study site (Figure 1) is located near Le Pellerin (upper estuary, 47°12,387; 1° 46,111) and benefits from continuous monitoring of dissolved oxygen in surface waters (SYVEL network).

The sampling site was visited four times, covering three contrasting hydrological settings. The first campaign occurred in August 2020 during an extreme low-water discharge period (LD, Figure 2) on board of RV Astérie. The monthly average Loire discharge (recorded at Montjean-sur-Loire; Hydro ID station: M530 0010 10) was only 130 m^3 s^{-1}, favoring TMZ presence at Le Pellerin. The second campaign took place during high discharge conditions (HD) in February 2021, during an exceptional flood event (up to 4,200 m^3 s^{-1}), following intense rainfall episodes (more than 90 cm of water per month fell in January and February 2020). The last two
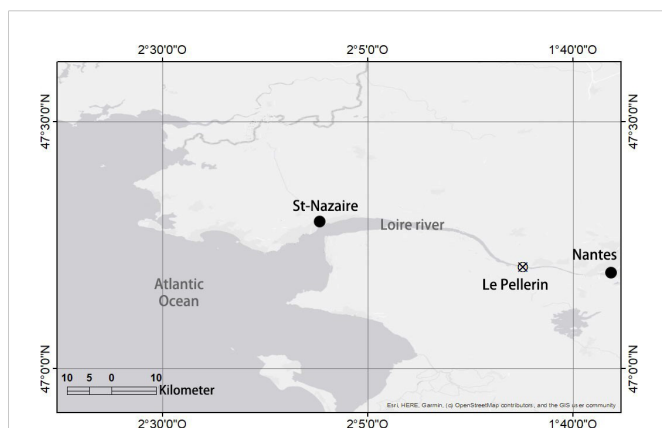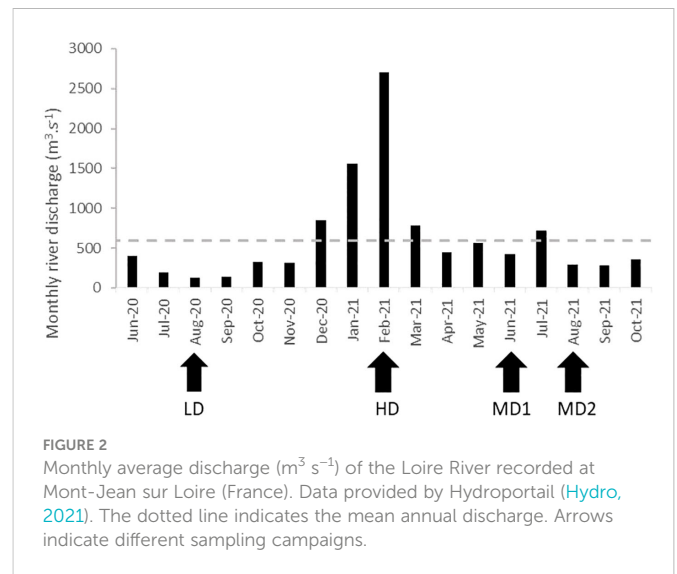

FIGURE 2
Monthly average discharge (m^3 s^{-1}) of the Loire River recorded at Mont-Jean sur Loire (France). Data provided by Hydroportail (Hydro, 2021). The dotted line indicates the mean annual discharge. Arrows indicate different sampling campaigns.

campaigns occurred during moderate-discharge periods in June (MD1) and August (MD2) 2021 (420 and 290 m^3 s^{-1}, respectively), sufficient to relocate the TMZ downstream from Le Pellerin. The three last campaigns were conducted aboard RVs Thalia and Côtes de la Manche (Metzger and Maillet, 2021) within the framework of REBELRED project.

2.2 Water and sediment sampling, processing, and analysis

During each campaign, temperature, salinity, and oxygen saturation of surface and bottom water (about 1m above the estuary floor) were measured using multiparameter HACH probes. Upon collection using a Niskin bottle, water samples were filtered and frozen prior to nutrient analysis. In the laboratory, ΣNH_3, NO_3^-, and dissolved phosphorus (P_d) concentrations were measured by segmented flow analysis using AA3 Seal Analytical according to the methodology of Bendschneider and Robinson (1952) optimized by Aminot et al. (2009).

In parallel, seven sediment cores were collected using a multicorer. The four cores were designated to incubations that were rapidly sealed and the oxygen concentration in the overlying water was maintained at the *in situ* oxygen concentration by bubbling ambient air and a N$_2$-400 ppm-CO$_2$ premix. Incubated cores were incubated in the dark at *in situ* temperature (± 0.1°C) while the overlying water was stirred constantly at 30 rpm using a Teflon-coated magnetic bar attached to the core lid (Pastor et al., 2011). Oxygen saturation was monitored during core incubations using a FireSting O$_2$ meter equipped with micro-optode and temperature probes (PyroScience GmbH). Overlying water was collected at the start and the end of the incubation period. The incubation duration and the sampling intervals of the overlying water were adjusted so that O$_2$ concentration in overlying water was never less than 80% of its initial value, which took 2 to 6 h. Overlying water samples were filtered through 0.2-μm Minisart® RC25 cellulosic syringe filters and separated into three different aliquots (dedicated to ICP AES analysis and nutrient and alkalinity measurements, see below). ΣNH_3, NO_3^-,

FIGURE 1
Map of the Loire estuarine region. The Le Pellerin sampling site is indicated by a crossed circle.

and P_d concentrations in the overlying water of the incubation experiments were measured using the same methodology as the water column analysis (see previous section). Alkalinity was determined by titration according to the Gran method using a Titrino (Metrohm GmbH), which also provides pH (Gran, 1952). A second aliquot of water was acidified to measure dissolved iron, manganese, and sulfate (Fe_d, Mn_d, and SO_4^{2-}) concentrations following the protocol for porewater analysis (Owings et al., 2019; see below).

One core was used for the determination of particulate organic carbon (POC) and radioisotope. The core was sliced every 1 cm and kept frozen until freeze-dried. An aliquot was decarbonated by exposure to HCl vapor (Lorrain et al., 2003) and analyzed using an Elemental Analyzer (NC2500, CarloErba). A second aliquot was dedicated to the determination of ^{210}Pb, ^{226}Ra, and ^{7}Be activities using a low background–high efficiency γ spectrometer (Schmidt et al., 2001). ^{7}Be values were corrected for radioactive decay that occurred between sample collection and counting. $^{210}Pb_{xs}$ was calculated as the difference of the measured ^{210}Pb and ^{226}Ra.

One core was designated to quantify the chemical composition of both porewater and dry sediment. The sediment was sliced in a N_2 purged glove bag into 2-mm slices for the first 2 cm, every 5 mm on the next 3 cm, then 10 mm up to 10 cm depth and finally in 20 mm slices for the rest of the core. Sediment slices were weighted and centrifuged (15 min at 3,500 rpm under N_2 atmosphere). Porewaters were filtered through 0.2-μm Minisart® RC25 cellulosic syringe filters and separated into different aliquots. One aliquot was acidified with a 1% equivalent volume of concentrated HNO_3 for ICP-AES analysis after a 10-fold dilution with a 1% HNO_3 solution. Total sodium, potassium, calcium, strontium, iron, phosphorus, manganese, and sulfur were measured. Elemental sulfur was interpreted as sulfate since sulfide is volatile and removed from the sample solution under acidic conditions (Metzger et al., 2007). A second aliquot was frozen until later analyses of dissolved nutrients ($\Sigma NH_3 = NH_3 + NH_4^+$, $NO_x = NO_2^- + NO_3^-$). NO_x concentrations were analyzed according to the Griess method, with vanadium chloride as nitrate reducer (Schnetger and Lehners, 2014). ΣNH_3 was analyzed according to the Berthelot method adapted to small samples with variable salinity (Metzger et al., 2019). The third aliquot was dedicated to the measurement of porewater alkalinity measurement according to the colorimetric method of Sarazin et al. (1999). The solid fraction was frozen and then freeze-dried. Porosity (Φ) was calculated from weight loss, assuming a particle density of 2.65 g cm^{-3} and a constant water density of 1 g cm^{-3} according to Eq. 1.

Equation 1:

$$\Phi = \frac{mH_2O \big/ \delta_{H_2O}}{\left(\frac{mH_2O}{\delta_{H_2O}} + \frac{m_{sed}}{\delta_{sed}} \right)}$$

where mH_2O and δ_{H_2O} are the mass and density of water, and m_{sed} and δ_{sed} are the mass and density of sediment (δ_{sed} = 2.65 g cm^{-3}). In consequence, the empty space due to possible cracks or burrows was not considered in the calculation of sediment porosity.

Metals associated to amorphous oxides (easily reducible by bacteria) were extracted from dry sediments following the ascorbate extraction procedure (Anschutz et al., 1998). Dry sediment (100 mg) was mixed with 10 ml of sodium bicarbonate (0.6 M), sodium citrate (0.17 M), ascorbic acid (0.11 M), and citrate solution (1M, pH 8) and gently stirred for 24 h. The supernatant was then filtered at 0.2 μm, stabilized with suprapur

HNO_3, and analyzed for Fe, Mn, and P, using an ICP-AES ICAP 6300 Thermo-Fischer. Vertical oxygen distribution was obtained on a designated core by microprofiling using 50-μm Clark-type microelectrodes (Unisense, Revsbech, 1989) mounted on a motorized micromanipulator. A linear calibration was performed between the in situ overlying water saturated with air at bottom temperature and zero oxygen in the anoxic part of the sediment. In situ temperature and oxygen saturation were maintained by bubbling both air and a N_2-400 ppm-CO_2 premix during profiling except for the MD1 campaign where overlying water was accidentally re-saturated. Overlying pH and oxygen conditions were monitored using static microsensors in the overlying water.

2.3 Water–sediment fluxes

Diffusive and total oxygen and nutrient fluxes at the sediment–water interface were assessed using two complementary approaches, calculated from porewater profiles and directly measured from sediment incubations. Diffusive fluxes were calculated from oxygen and nutrient profiles according to Fick's first law (Fick, 1855), adapted by Berner (1980):

Equation 2:

$$J_{diffusive} = -\Phi D_s \frac{dC}{dx}$$

where Φ is the porosity and $D_s = D_{mol}/\theta^2$ is the sediment diffusivity coefficient calculated from the molecular diffusion coefficient D_{mol} (Berner, 1980) established for each solute species as an empirical function of temperature and salinity (using "marelac" R package; R Core Team, 2013). The tortuosity θ^2 is typically taken as a function of the porosity, as in the modified Weissberg relationship, $\theta = 1–2 \ln(\Phi)$.

Total oxygen and nutrient fluxes were estimated from the linear decrease of oxygen or nutrient concentrations in the overlying water of each sediment core incubated in a closed layout (Bowman and Delfino, 1980), according to Equation 3.

Equation 3:

$$J_{total} = slope \star V_{water} / S_{sediment}$$

$$J_{total} = slope \star H_{water}$$

where slope is the slope of the linear decrease of dissolved oxygen or the nutrient concentration difference from start to end in the overlying water of the incubated sediment. Dissolved oxygen concentration was calculated considering oxygen saturation, temperature, salinity, and barometric pressure. V_{water} is the volume of overlying water and $S_{sediment}$ is the surface of sediment evaluated from internal radius R of the sediment core ($S = \pi \star R^2$; $R = 4.8$ cm) and H_{water} is the overlying water height.

2.4 Mass balance and sediment contribution to hypoxia

The contribution of sediments to the overlying water column stock was integrated in the downstream part of the estuarine, delimited by the location of St-Nazaire and Nantes. The

characteristic time ($\tau_{sed,x}$) of O_2, NO_3^-, ΣNH_3, and P_d was studied according to estuarine sediment fluxes and water residence times estimated using Eq. 4 (Centre national pour l'exploitation des océans, 1984):

Equation 4:

$$T_{residence} = Age_{Water,\ Saint-Nazaire} - Age_{Water,\ Nantes}$$

where $Age_{water,\ Saint-Nazaire}$ and $Age_{Water,\ Nantes}$ are the relative ages of water estimated from Montjean sur Loire station according to the Loire discharge intensity Q (in $m^3\ s^{-1}$).

$$Age_{water,\ Saint-Nazaire} = \frac{65*10^3}{Q} * e^0$$

$$Age_{water,\ Nantes} = \frac{65*10^3}{Q} * e^{-0.04*63}$$

The characteristic time $\tau_{sed,x}$ corresponds to the half-life (or half-doubling time) in case of progressive consumption (or production) of dissolved species x in the estuary, regardless of its concentration; $\tau_{sed,x}$ is calculated using Eq. 5:

Equation 5:

$$\tau_{sed,\ x} = \left| \frac{Stock_x}{2*J_{total,\ x}} \right|$$

where $Stock_x$ is the amount of the dissolved species x before sediment consumption or production. In this preliminary approach, we assume that the sediment flux only comes from the muddy sediments of the downstream Loire estuary and that the flux obtained at Le Pellerin is constant over all the muddy sediment surface and is representative of this system, according to:

Equation 6:

$$\tau_{sed,\ x} = \left| \frac{C_x * Depth_{water} * S_{estuary}}{2*J_{total,x} * S_{estuary} * \%_{mud}} \right|$$

$$\tau_{sed,\ x} = \left| \frac{C_x * Depth_{water}}{2*J_{total,x} * \%_{mud}} \right|$$

C_x is the concentration of the solute x (in µM) in surface waters upstream of the studied estuarine section (Nantes). $Depth_{water}$ is the mean monthly water depth (in m) recorded at Le Pellerin (data provided by REFMAR SHOM service). $J_{total,x}$ is the total flux of solute x from the sediment compartment evaluated by the incubations. $S_{estuary}$ and $\%_{mud}$ are respectively the total subtidal surface (5.2×10^7 m^2) and the proportion occupied by muddy sediment (62%). The boundary conditions set for each campaign (LD, HD, MD1, and MD2) are given in the Supplementary Data section.

The water column contribution to DO, $\Sigma NH_3 + NO_x$, and P_d budget was estimated using the biological oxygen demand after 5 days of incubation (BOD_5); data are available in the NAIADE database (www.naiades.fr). The given solute characteristic time toward water reactivity ($\tau_{water,x}$) is thus calculated assuming a regular consumption of oxygen according to Eq. 7:

Equation 7:

$$\tau_{water,\ x} = \frac{C_x * V_{estuary}}{2 * \frac{BOD_5}{5} * V_{estuary} * \gamma^x}$$

$$\tau_{water,\ x} = \frac{C_x}{2 * \frac{BOD_5}{5} * \gamma^x}$$

where γ^x is the stoichiometry of the solute reaction during aerobic respiration (Soetaert et al., 2007), i.e., $\gamma^{O2} = 1$, $\gamma^N = 0.156$, and $\gamma^P = 0.0094$. $V_{estuary}$ is the volume of water in the internal estuarine section (during low-tide period).

This simple model also allows us to estimate the fraction of the initial upstream stock of a solute that is consumed or produced within the estuary:

Equation 8:

$$f_{cons,\ water,\ x} = \frac{\tau_{water,\ x}}{2 * T_{residence}} \quad \text{and} \quad f_{cons,\ sed,\ x} = \frac{\tau_{sed,\ x}}{2 * T_{residence}}$$

3 Results

3.1 Water column chemistry

Sampling cruises occurred during different seasons, as shown by water temperature ranging from 9.88 (February 2021, HD) to 23.4°C (August 2020; LD) (Table 1). Salinity was usually low (0.11–0.30), except in August 2020 (1.34, LD). Dissolved oxygen (DO) concentration and saturation in the water column ranged from 80 µM and 29.8% (LD) to 308 µM and 87.3% (HD). A moderate hypoxia was only observed in August 2020 (LD) and a small DO depletion affected bottom water in June 2021 (MD1; 64.5%). Surface nitrate and nitrite (NO_x) concentrations were minimal during the extreme low-discharge period (68 µM, LD) and maximal during flood (253 µM, HD). A noticeable difference between surface and bottom NO_x concentrations was only observed during LD with a bottom concentration of only 3.8 µM. By contrast, ΣNH_3 concentrations remained rather low, from 0.1 (MD2) to 22 µM (LD), whatever the sampling period. P_d was undetectable in February (HD) and remained relatively low and stable, ranging from 1.14 to 1.68 µM, during the other surveys.

3.2 Sediment characteristics

Profiles of porosity, dry bulk density, POC, $^{210}Pb_{xs}$, and ^7Be as a function of depth in sediment are shown in Figure 3. The activity of $^{210}Pb_{xs}$ was relatively constant over depth and across the different seasons ranging from 86 to 124 mBq g^{-1}. Porosity at the top of the cores ranged from 0.84 (MD1) to 0.94 (LD). In August 2020 (LD), the uppermost 2-cm sediments showed high porosity and ^7Be activity of about 40 mBq g^{-1}, associated with a POC of about 2.8 ± 0.1%. Below, porosity and ^7Be decreased to reach 0.88 at 20 cm depth and negligible activity below 10 cm, respectively, while POC increased up to 3.4%. In February 2021 (HD) sediment surface was cracked and showed intense bubbling activity (Figure 4), generating empty spaces along the cores that could not be quantified for porosity. Porosity showed a maximum of 0.87 at 1 cm depth corresponding to a POC of 3.1% and porosity decreased downward to reach 0.83 at 19 cm depth. POC profile was relatively noisy, approximately 3.0 ± 0.3% down to 9 cm depth, then steadily decreased to 2.8% at 25 cm depth. ^7Be activity was always below the

TABLE 1 Physical and chemical properties of surface and bottom waters at Le Pellerin.

Station	Date	Water column layer	T (°C)	Salinity	O₂ sat (%)	O₂ (µM)	ΣNH₃ (µM)	NOₓ (µM)	Pd (µM)
LD	08/2020	Surface	22.3	1.26	29.8	80	1.4	68	BQL
LD	08/2020	Bottom	22.2	1.34	29.8	80	0.1	62	BQL
HD	02/2021	Surface	9.88	0.11	87.2	307	4.6	253	1.22
HD	02/2021	Bottom	9.88	0.11	87.3	308	NA	NA	NA
MD1	06/2021	Surface	21.8	0.16	84.1	230	7.2	159	1.53
MD1	06/2021	Bottom	20.5	0.19	64.5	181	22	146	1.19
MD2	08/2021	Surface	23.4	0.30	78.0	207	0.6	165	1.14
MD2	08/2021	Bottom	23.4	0.30	74.0	196	0.7	162	1.68

Bottom water column samples were collected approximatively 1 m above the estuarine floor. Due to a sampling issue caused by the high discharge during the HD survey, nutrient concentrations of bottom water were not determined. BQL, Below quantification limit; NA, not analyzed.

detection limit. In June 2021 (MD1), sediment surface was still cracked and porosity was rather constant. Finally, in August 2021 (MD2), topcore cracks were completely filled. The porosity profile was similar to the one recorded in August 2020, with a rapid decrease in the first centimeters (0.88 to 0.85) and stabilization below (0.85 ± 0.07). A moderate ^{7}Be activity (20 mBq g^{-1}) was measured only in the upper centimeter.

3.3 Oxygen distribution at the sediment–water interface

Dissolved oxygen penetration depth (OPD) in sediments ranged from 0.13 ± 0.02 to 0.24 ± 0.02 cm (Figure 5). The OPD reached a maximal value during LD, a minimal value during MD2, and
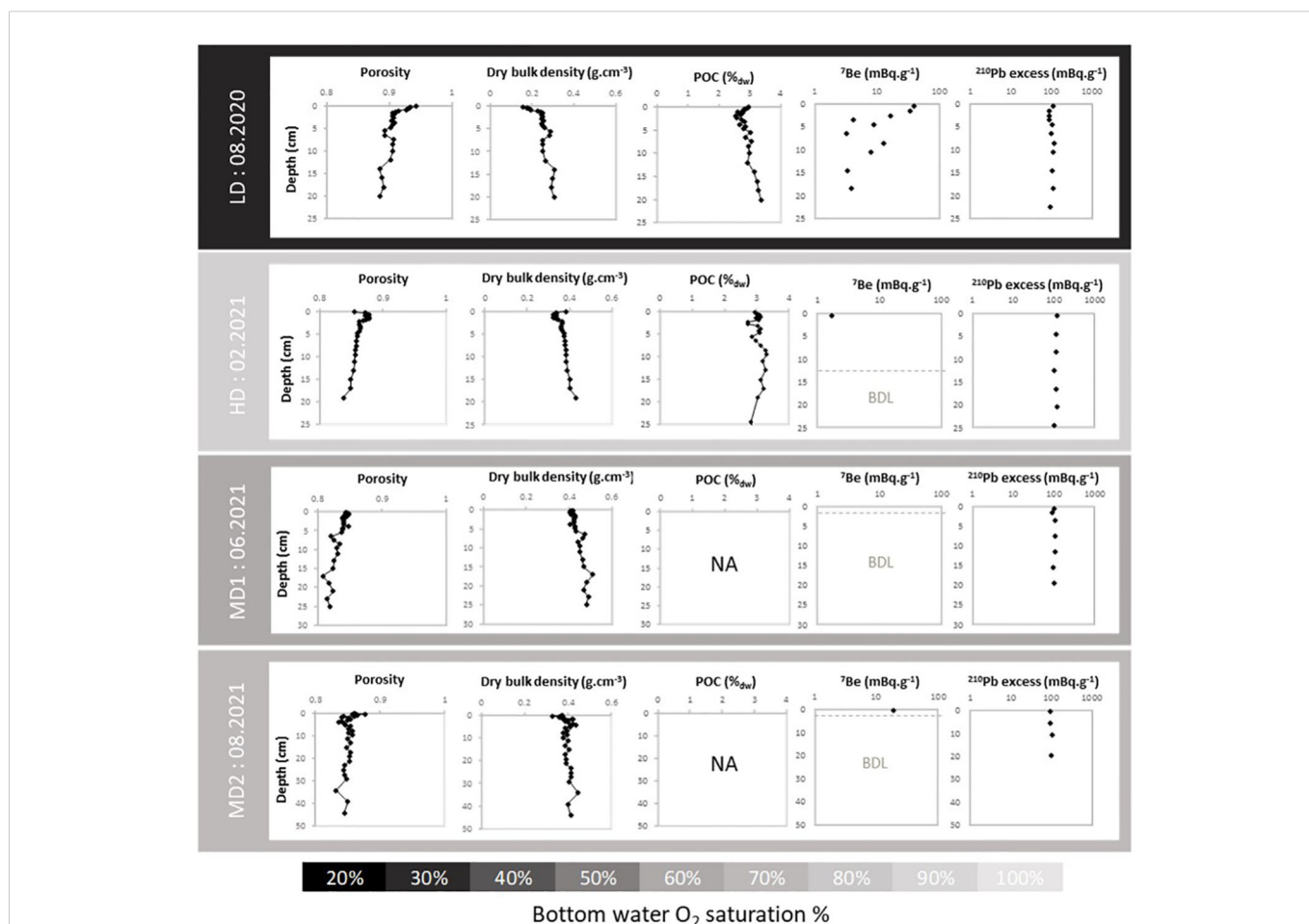

FIGURE 3
Profiles of porosity, dry bulk density (g*cm^{-3}), particulate organic carbon (%), and ^{7}Be and ^{210}Pb$_{xs}$ activities (mBq g^{-1}) with depth in sediment at Le Pellerin. BDL, below detection limit; NA, not analyzed.

FIGURE 4
Photos of topcore sediments collected during HD and MD1 campaigns: deep cracks (left and middle panels) and gas accumulation in the cracks (right panel) are visible.

intermediate and similar values during HD and MD1. During summer 2020 (LD1), the profiles were very reproductible and showed a typical exponential decrease, while for the other campaigns, a higher shape heterogeneity was observed between profiles, especially during winter (HD) and late spring (MD1). It should be noted that during the MD1 campaign, deoxygenation was measured in overlying waters, but micro-profiling was accidently done at atmospheric oxygen saturation.

3.4 Redox-sensitive elements from interface cores

Dissolved and particulate redox-sensitive reactive elements of porewaters are depicted in Figure 6. Arrows indicate dissolved

concentrations of the overlying water. Ammonia species were below 10 μM in overlying waters for all cores. During the LD survey, ΣNH_3 concentration increased linearly with depth up to 1.0 mM at the maximum sampled depth (20 cm). During the HD survey, ΣNH_3 increased rapidly within the top 5 cm and remained stable below at 1.8 mM. During the MD1 and MD2 surveys, ΣNH_3 gradient was smoother near sediment water interface (SWI) with a plateau reached at 20 cm depth with concentrations of 3.9 mM for MD1 and 2 mM for MD2. Nitrate showed opposite trends with high concentrations in the overlying waters (below 70 μM for LD, HD, and MD2 and above 100 μM for MD1) and a rapid decrease in porewaters with depth. During the flood, porewater nitrate was low but rather constant in the first 25 mm. During LD, MD1, and MD2, the decrease in nitrate was more progressive with a total disappearance at 20, 9, and 13 mm, respectively.
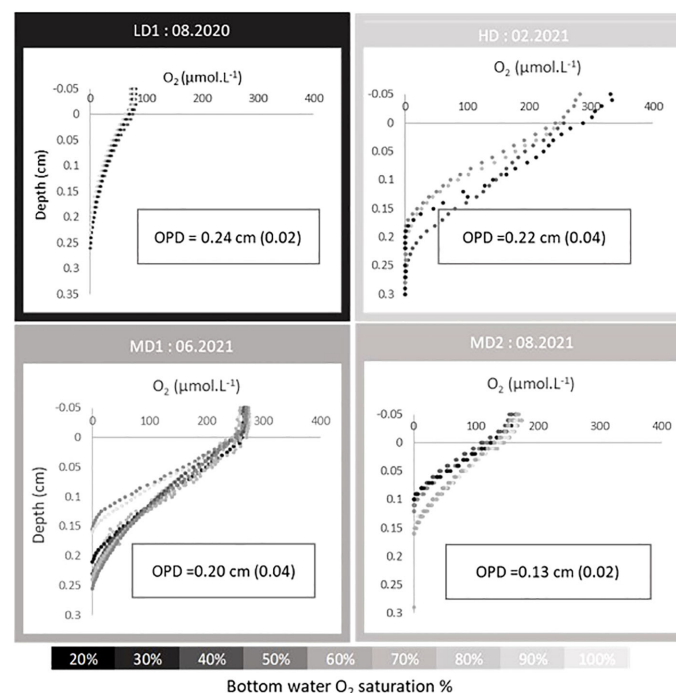

FIGURE 5
Oxygen profiles through sediment−water interface and respective oxygen penetration depth (mean and standard deviation) for the different campaigns at Le Pellerin. *In situ* temperature and oxygen saturation were maintained during profiling except for the MD1 campaign where overlying water was accidentally re-saturated.
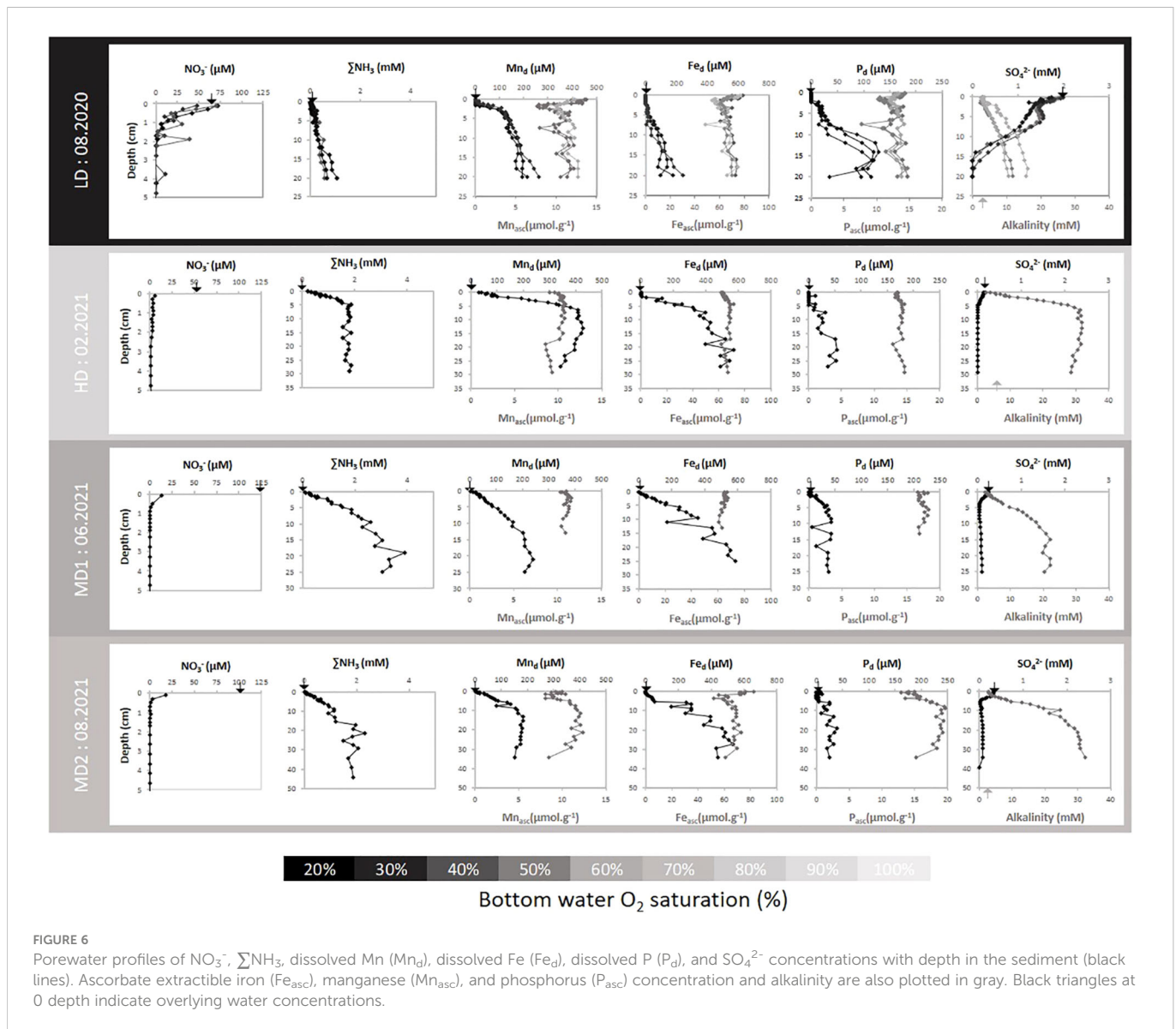
FIGURE 6
Porewater profiles of NO_3^-, $\sum NH_3$, dissolved Mn (Mn_d), dissolved Fe (Fe_d), dissolved P (P_d), and SO_4^{2-} concentrations with depth in the sediment (black lines). Ascorbate extractible iron (Fe_{asc}), manganese (Mn_{asc}), and phosphorus (P_{asc}) concentration and alkalinity are also plotted in gray. Black triangles at 0 depth indicate overlying water concentrations.

Fe and Mn production in the porewaters was observed for all campaigns. In summer 2020 (LD), Mn_d increased with the decrease of NO_3^- in the top 2 cm and reached a maximum at 270 µM. Fe_d increased from 5 cm depth to reach 240 µM at the bottom of the core. At this period, Fe_{asc} and Mn_{asc} showed a maximum in the surface sediment (with 77 and 13 µmol g^{-1}, respectively) followed by a minimum at 2 cm depth (56 and 7.6 µmol g^{-1}, respectively) and an almost stable concentration below. During winter 2021 (HD), Mn_d increased sharply from 0 to 7 cm depth reaching up to 420 µM while Fe_d increased mostly within the 2–10 cm depth layer up to 570 µM. In contrast to the LD period, no surface accumulation of Fe_{asc} and Mn_{asc} was observed, but a minimum concentration. Four months later (MD1), Fe_{asc} and Mn_{asc} surface depletion had vanished. Mn_{asc} and Fe_{asc} showed almost no vertical gradient. Mn_d exhibited a less sharp profile than previously with a maximum concentration reaching only 240 µM in the deepest sediment layers. Fe_d increased almost linearly with depth, maintaining high concentrations at the bottom of the core (up to 580 µM). Finally, during summer 2021 (MD2), surface accumulation of Fe_{asc} and Mn_{asc} was again visible at the surface (82 and 10 µmol g^{-1}, respectively). Below,

Fe_{asc} and Mn_{asc} remained approximately 55 and 8.1 µmol g^{-1}, respectively. Deep Mn_d and Fe_d remobilization was roughly similar to MD1 survey with maximum concentrations of 530 µM and 180 µM for Fe_d and Mn_d at 20 cm depth.

Production of dissolved phosphorus P_d was visible during all surveys and generally observed below 5 cm depth. One can observe that P_d production was particularly intense during summer 2020 (reaching 128 µM at 15 cm, LD) compared to the other sampling times. For all surveys, surface concentration of P_d was zero as a result of important bounding control from oxides. Most differences between surveys were attributed to P_{asc} behavior. Similar to the Fe_{asc} and Mn_{asc} profiles, the P_{asc} profile showed significant accumulation at the surface sediment layer during summer 2020 (maximum concentration reaching 14.3 µmol g^{-1}), a small depletion during winter 2021 (minimal concentration of 13.5 µmol g^{-1}), and no vertical gradient during June 2021 (rounding 17.2 µmol g^{-1}). Contrasting with oxides' profile, P_{asc} concentration showed a high depletion at the top most sediment during August 2021 (MD2) with minimal concentration reaching 12.8 µmol g^{-1}.

The highest concentrations of sulfate are observed in the overlying waters, according to riverine discharge (LD showed the highest concentration of 2 mM, while other surveys showed concentrations below 0.5 mM). Downcore, sulfate decreased until reaching the detection limit (below 15 cm depth for LD and approximately 5 cm depth for HD, MD1, and MD2). In spring (MD1) and summer 2021 (MD2), sulfate was detected below 5 cm depth, showing a slight increase toward the bottom of the cores.

For all surveys, alkalinity increased with sediment depth. Moreover, a significant fraction of alkalinity seemed to be produced concomitantly with the sulfate consumption zone. During summer 2020 (MD2), alkalinity increased quasi-linearly with depth (reaching 16.4 mM). During the other surveys, alkalinity profiles were more steep. During winter 2021 (HD), most alkalinity production was completed in the upper 10 cm, reaching 31.5 mM. During June 2021 (MD1), alkalinity production continued down to 15 cm depth, reaching 22 mM. Finally, during August 2021 (MD2), alkalinity production was still visible, reaching 32 mM down to 34 cm depth.

3.5 Water–sediment fluxes

Figure 7 illustrates the variability of oxygen and nutrients' residence time as a function of water residence time within the estuary if sedimentary uptake is taken into account (Table 2) or if water column oxygen demand is used (see numbers in Appendix 2 and Appendix 3). Oxygen exchange between sediment and water column was relatively low during the low-discharge period (8.1 and 24 mmol m^{-2} day^{-1} for diffusive and total fluxes, respectively, Table 2). The extremely high residence time of estuarine water due to low water discharge in summer 2020 (LD, 18.7 days) allows a moderate sedimentary oxygen uptake to consume 31% of the oxygen estuarine stock (Figure 7A). In parallel, water column oxygen uptake accounted for 50% of the total consumption (Figure 7B). Observed DO saturation (30%) was higher than predicted by this simple model (15%) during LD period. At this period, a significant diffusive flux of nitrate into the sediment was observed (0.8 mmol m^{-2} day^{-1}), resulting in a positive nitrogen sediment budget (due to low efflux of ΣNH_3 during the LD period). For the same conditions, benthic diffusive phosphorous fluxes were below quantification limit. In the absence of neither upstream nutrients information nor total nutrient flux values, characteristic times for nutrients were not calculated.

Six months later, extreme sediment oxygen demand (up to 94 mmol m^{-2} day^{-1}) was recorded during the flood high-discharge period (HD, $Q = 4200$ m^3 s^{-1}). Total:diffusive flux ratios were particularly high for oxygen and other solute species (e.g., $J_{total, oxygen}$:$J_{diffusive,oxygen}$ = 7.2). Strong nitrogen efflux was observed at the surface sediment from incubation experiments (−12 and −44 mmol m^{-2} day^{-1}, respectively, for NO$_3$ and ΣNH_3). Similarly, total P$_d$ efflux was maximal during the HD period reaching −1 mmol m^{-2} day^{-1}. At this date, water-residence time was particularly short (0.9 day) and water–sediment exchanges demonstrated low capability to affect pelagic oxygen stock ($f_{sed,O2}$ = −4%; $f_{water,O2}$ = −3%). ΣNH_3 was the most affected nitrogen species by sediment and water reactivity. The water column ΣNH_3 stock would be doubled ($f_{sed, \Sigma NH3}$ = 222%) under observed sediment nitrogen efflux (Table 2 and Figure 7), indicating that most of the ΣNH_3 observed in the water column (3.5
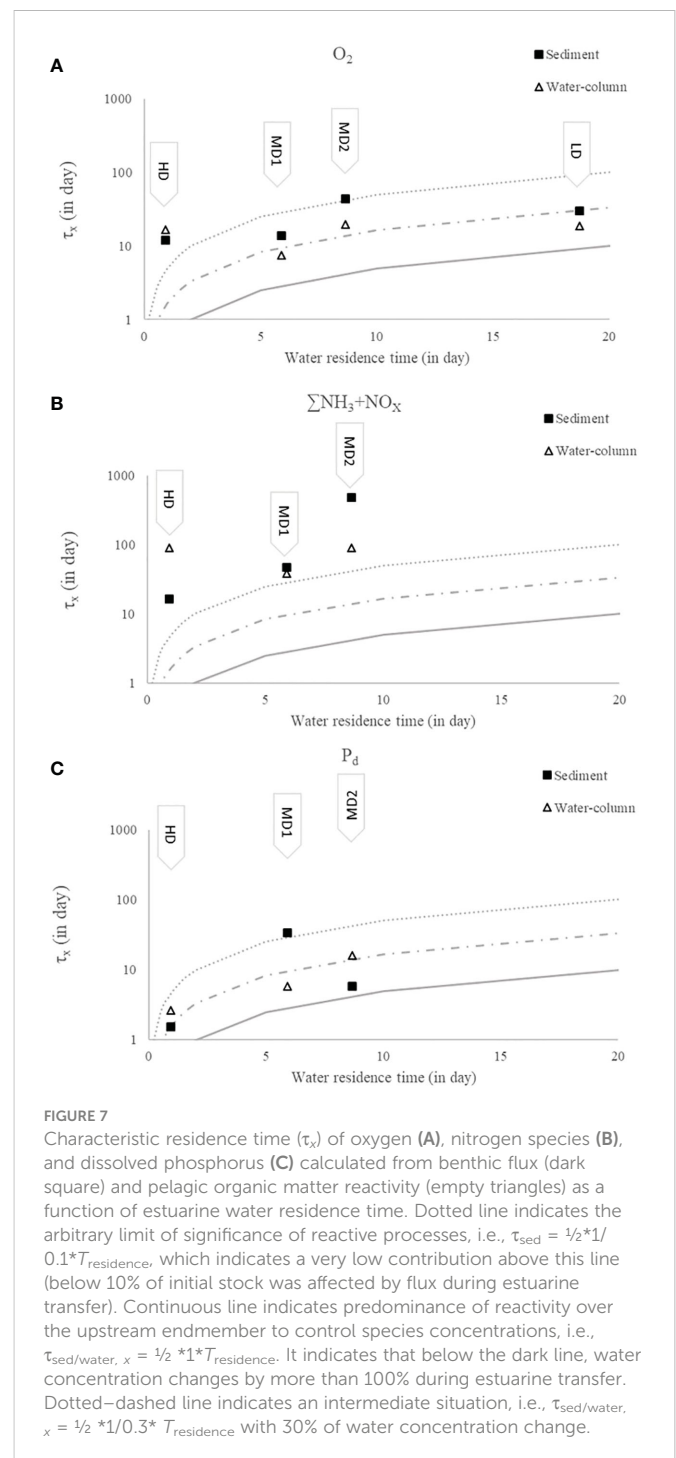

FIGURE 7
Characteristic residence time (τ_x) of oxygen (A), nitrogen species (B), and dissolved phosphorus (C) calculated from benthic flux (dark square) and pelagic organic matter reactivity (empty triangles) as a function of estuarine water residence time. Dotted line indicates the arbitrary limit of significance of reactive processes, i.e., $\tau_{sed} = ½*1/0.1*T_{residence}$, which indicates a very low contribution above this line (below 10% of initial stock was affected by flux during estuarine transfer). Continuous line indicates predominance of reactivity over the upstream endmember to control species concentrations, i.e., $\tau_{sed/water, x} = ½ *1*T_{residence}$. It indicates that below the dark line, water concentration changes by more than 100% during estuarine transfer. Dotted–dashed line indicates an intermediate situation, i.e., $\tau_{sed/water, x} = ½ *1/0.3* T_{residence}$ with 30% of water concentration change.

μM) could result from sediment effluxes. By release of P$_d$, the sediment would also increase water column P$_d$ stock by 30% (Table 2), while contribution of the water column was negligible for all nutrients and oxygen stocks.

Four months after the flood (MD1), water discharge was about 422 m^3 s^{-1} and temperature was high (>20°C). Benthic fluxes decreased simultaneously with a sediment oxygen uptake of 47 mmol m^{-2} day^{-1} that maintained an important $J_{total,oxygen}$:$J_{diffusive, oxygen}$ ratio (1.7). Taking into account a water residence time of 5.90 days for this period, such sediment consumption would allow a decrease of 21% of the oxygen stock, much lower than the $f_{water,O2}$ = −39% consumption from water column respiration. The O$_2$

TABLE 2 Average total and diffusive fluxes of O_2, NO_3^-, $\sum NH_3$, and P_d at the sediment–water interface.

	O_2	NO_3^-	$\sum NH_3$	P_d
	mmol m^{-2} day^{-1}	mmol m^{-2} day^{-1}	mmol m^{-2} day^{-1}	mmol m^{-2} day^{-1}
LD				
Diffusive	8.1 (0.7)	0.8 (0.3)	−0.5 (0.4)	0.0 (0.2)
Total	24 (3.0)	NA	NA	NA
$f_{sed,x}$	−31%			
HD				
Diffusive	13 (2)	0.01	−3.4	BQL
Total	94 (20)	−12 (24)	−44 (16)	−1 (1)
$f_{sed,x}$	−4%	−1%	+222%	+30%
MD1				
Diffusive	22 (3.6)	0.3	−3.7	BQL
Total	47 (30)	3.7 (6.6)	−15 (28)	0.1 (0.3)
$f_{sed,x}$	−21%	−2%	+193%	−9%
MD2				
Diffusive	18 (2.9)	1.0	−0.60	BQL
Total	17 (1.8)	3.1 (9.5)	−2.0 (14)	1.0 (1.5)
$f_{sed,x}$	−10%	−3%	+16%	−75%

Negative numbers indicate fluxes from sediment towards water column. Standard deviation was indicated in brackets. $f_{sed,x}$ corresponds to fraction of solute stock affected by sediment fluxes. BQL, Below quantification limit; NA, not analyzed.

saturation measured at Le Pellerin was about 65%, much higher than predicted by the model (40%). Variability between cores was noticeable during the incubation experiment (e.g., observed TOU ranged from 22 to 90 mmol m^{-2} day^{-1}). Despite significant variability, sediment again contributed to consume NO_3^- (3.7 mmol m^{-2} day^{-1}) and release $\sum NH_3$ (−15 mmol m^{-2} day^{-1}). Finally, MD1 observations showed again very low P_d fluxes (0.1 mmol m^{-2} day^{-1}). During this survey, only $\sum NH_3$ stock was significantly affected by sediment–water exchanges, with more than 193% of $\sum NH_3$ water column standing stock increase under sediment influence.

Six months after the flood, during the second summer campaign (MD2), all water–sediment fluxes showed minimum values concomitant with a decrease of the J_{total} : $J_{diffusive}$ ratio. Total sediment oxygen flux was at a minimum reaching only 17 mmol m^{-2} day^{-1}. Sediment oxygen flux during summer 2021 (MD2) accounted only for 10% of the O_2 stock decrease along 8.7 days of estuarine water residence, half as much as the water column oxygen consumption that was responsible for 22% of O_2 stock decrease (Table 2). Again, predicted oxygen saturation (68%) by model was lower than oxygen saturation measured at Le Pellerin (76%). The difference was mostly attributed to non-apprehended water–atmospheric exchange, especially re-aeration of water oxygen stock. At this moment, the nitrogen budget for sediment was almost in balance due to low NO_3 consumption (3.1 mmol m^{-2} day^{-1}) and a minimal $\sum NH_3$ benthic efflux (−2.0 mmol m^{-2} day^{-1}). A noticeable exception from the general decrease of sediment–water fluxes was observed for the total P_d influx towards the sediment reaching 1.0 mmol m^{-2} day^{-1} total during the last MD2 survey. Benthic P_d uptake was responsible for 75% of the water column P_d decrease due to the

low initial stock of P_d in the water column and its high water residence time (8.7 days).

4 Discussion

4.1 Extreme hydrologic conditions and their benthic geochemical signature

During the low fluvial discharge campaign in August 2020 (LD; 133 m^3 s^{-1}), the Loire River showed an important saline intrusion that promoted the presence of the TMZ and a subsequent sediment deposition at Le Pellerin. This recent deposit corresponded to a weakly consolidated mud enrichment in ^{7}Be ($\tau_{1/2 =}$ 53 days) and in particulate organic carbon (POC) up to 3% (Figure 3), which corresponded to the average POC content of suspended materials in the Loire estuary (Etcheber et al., 2007). This deposit is likely to be resuspended when riverine discharge will increase (Ross and Mehta, 1989). Below, the older deposit layer was characterized by erratic isotopic, porosity, and POC signatures, which indicates a less regular deposition. This stochastic deposition was most likely the result of higher tidal and Loire discharge energy coupled with an intense sediment deposition–resuspension process acting in the estuary during the rest of the current year as ^{7}Be was still detected.

Six months later, during the flood, the Loire River discharge exceeded 4,200 m^3 s^{-1} (according to historical records, a returning phenomenon of an instantaneous discharge of 4,000 m^3 s^{-1} with a periodicity of 4 years), which is twice the critical threshold for sediment destabilization calculated by rheological studies (Sanchez

and Levacher, 2008). Important erosion of surface sediments exposing older sediment was demonstrated by the absence of ^{7}Be in surface sediments. Exposed sediments were deep dark, very cohesive, and compacted. Their geochemical signatures were characterized by low iron and manganese oxide concentrations with an absence of enrichment in the shallower depths of sediment. Mean values for oxide concentrations were similar to the buried oxide concentrations previously observed during the low discharge survey (65 and 9 μmol g^{-1} for iron and manganese oxides, respectively). Sediments also showed important ebullition with bubbles large enough to generate slabs of sediments that could be tilted upside down. As a result, sediment was full of cracks and centimeter-large empty spaces (Figure 4), favoring non-diffusive transportation of solutes that dominated benthic exchanges with incubation fluxes much higher than diffusive ones (see HD results in Table 2). Progressively, crack walls observed during flood period (HD) were oxidized (MD1) and eventually filled with new material from the TMZ, late August (MD2).

4.2 Influence of extreme hydrological conditions on diagenetic processes and benthic fluxes

During the low-discharge period, surface sediments of Le Pellerin were periodically exposed to TMZ and bottom water hypoxia. Within the sediment, OM mineralization was relatively low (the lowest diffusive oxygen flux was recorded in the low discharge survey; Table 2) and mostly caused by anaerobic processes (most ΣNH_3 production was occurring in deeper in the sediment). The high Fe$_{asc}$ and Mn$_{asc}$ oxide content of eroded material from the Loire catchment area allowed important reductive dissolution below OPD (Figure 6). Dissolved Fe$_d$ and Mn$_d$ produced by oxide dissolution diffused upward and were re-oxidized, leading to an accumulation of oxides in the surface layer and no diffusive flux out of the sediment (Figure 6). Maintenance of an oxide-enriched layer in the upper centimeters despite hypoxic exposure contradicts general coastal and estuarine reports of massive iron and manganese dissolution during water column hypoxia events (Kristiansen et al., 2002; Lenstra et al., 2021). This contradiction can be explained by oxidation of Fe$_d$ and Mn$_d$ due to the high concentration of NO_3^- within the sediment (Luther et al., 1997; Jamieson et al., 2018), which was measured during the low discharge campaign and confirmed by its significant consumption within the sediment (0.9 mmol m^{-2} day^{-1}). Multiple studies in lakes, salt marshes, or other aquatic contexts already highlighted the coupling between NO_3^- and metal remobilization from the benthic compartment (Hansen et al., 2003; Burgin et al., 2011; Moncelon et al., 2021; Moncelon et al., 2022). The persistence of iron and manganese oxides despite hypoxic conditions prevents phosphorus to be released out from the sediment, generating an important phosphorus storage through adsorption onto iron oxides (P$_{asc}$/Fe$_{asc}$ between 0.17 and 0.20; see Appendix 4), and reaching the highest values of previous observations on Loire intertidal mudflats (Thibault de Chanvalon et al., 2016). This phosphate accumulation limits the sediment contribution to water column eutrophication and subsequent hypoxia. Indeed, P$_d$ is the limiting nutrient in the Loire estuary as indicated by its complete consumption in the water column (below detection limit, Table 1).

Paradoxically, the HD campaign of February 2021 was characterized by low OM mineralization rates associated with high benthic fluxes (Table 2). Alkalinity and ammonium showed very large gradients, which induced high diffusive fluxes. These species are usually good indicators of anaerobic mineralization processes. However, most of the variability of these species was correlated to the variability of Na and Li indicating that benthic diffusive fluxes were driven by mixing and not by mineralization processes. During the flood, benthic compartment contributed to an intense sediment oxygen demand (94 mmol m^{-2} day^{-1}) coupled with the release of ΣNH_3, NO_3^-, and P$_d$ (−12, −44, and −1 mmol m^{-2} day^{-1}, respectively). To complete our picture of dissolved species benthic release, the vertical gradient of Mn$_d$ concentration underlines the existence of Mn$_d$ diffusive efflux from the sediment and a strong control of Fe$_d$ in the top layers of sediment during this period (Figure 6). The paradoxical high sedimentary effluxes, despite low mineralization rates, can be explained by the erosion of recent deposit stripping older sediments rich in dissolved species. In addition, intense gas ebullition associated with centimeter long openings (Figure 4) stimulated convective transport, increasing the $J_{total,oxygen}$:$J_{diffusive,oxygen}$ ratio up to 7. Several studies demonstrated that the increase in gas partial pressure combined with depressurization due to erosion generates catastrophic ebullition that creates fracking in cohesive sediments (Algar et al., 2011a; Algar et al., 2011b), which allowed for increase of gas and solute water–sediment exchanges (Cheng et al., 2014; Flury et al., 2015). The upstream location of the station combined with the flood supports the hypothesis of methane degassing, as little sulfate is present to be respired and to oxidize methane diffusing from depth (Borges and Abril, 2011). Methane oxidation by oxygen may also contribute significantly to the observed large total oxygen consumption. Moreover, an examination of microbial diversity revealed the presence of methanogenic bacteria on the surface sediment (unpublished data). High methane concentrations were previously reported in the upper part of the Loire estuary during flood (Middelburg et al., 2002), strengthening our assumption of methane bubbling during the 2021 flood. Within the sediment (Figure 6), iron oxide dissolution below the sulfate consumption zone (0 to 5 cm) could be produced by anaerobic oxidation of methane (AOM; Yang et al., 2021). Advection through cracks combined with the absence of reactive metallic oxides eroded by the flood may have favored dissolved phosphorus exchanges (Table 2). However, an obvious variability was observed between replicates during incubation, which is probably caused by heterogeneity in the distribution of cracks on the mud surface and bubbling randomness.

4.3 Sedimentary resilience after the flood

After winter flood, the Loire discharge decreased favoring upstream migration of TMZ and associated deposition. During late June 2021 (MD1), 4 months after the flood, partial filling of the fractures on the sediment surface inherited from the flood was visually observed. (Figure 4). Conversely to the low-discharge period, the recent deposited layer was only few mm thick and composed of old sediment, explaining the absence of ^{7}Be activity at the surface of sediment (Figure 3). Unfilled cracks showed an oxidized layer along their walls, suggesting that those cracks were relatively (probably 4 months) old. Diffusive oxygen flux was higher than before (13 and 22 mmol m^{-2} day^{-1} observed during HD and MD1

respectively; Table 2), indicating increased mineralization processes, probably due to the higher temperature (from 9.88 to 20.5°C). Deep ΣNH_3 production suggests that the main part of mineralization processes was completed by anaerobic pathways. At sediment surface, ΣNH_3 diffusive benthic fluxes remained in the same order (3.7 versus 3.4 mmol m^{-2} day^{-1} for winter flood; Table 2). Moreover, the total sedimentary influx of oxygen and efflux of ΣNH_3 were divided by 2 and 3, respectively, compared with the flood period (Table 2). Indeed, partial filling of the cracks and decreased ebullition, although still active during the MD1 incubation experiments, strongly reduced the convective and advective transport, decreasing the total by diffusive flux ratio from 7 and 13 to 2 and 4, for oxygen and ΣNH_3 respectively. NO_3^- and P_d diffusive fluxes remained low or below the quantification limit while total fluxes were quite variable with opposite directions among replicates showing the competition between diffusive and non-diffusive exchanges. Supported by Fe_d and Mn_d vertical gradients, significant metal efflux from sediment was observed during this period. We suspect that metal dissolution was associated with the exposure of Fe_{asc} and Mn_{asc} to CH_4 and the low NO_3^- control in porewater.

In August 2021, 6 months after the flood event (MD2), the cracks previously generated by gas ebullition were almost completely filled with sediment. Oxygen and nutrient benthic were at a minimum, close to the low discharge (LD) value for oxygen, as a consequence of the end of ebullition processes and the decrease in exchange surface area. Total fluxes were equal to diffusive fluxes for oxygen, the closest being for ΣNH_3 and NO_3^- (Table 2). Within the surficial sediment layer, Fe_{asc} and Mn_{asc} showed significant accumulation similar to during the low-discharge period, despite both being actively remobilized deep within the sediment. Curiously, diffusive metal release was stopped at the sediment surface despite repeated exposition to hypoxic conditions. Near SWI, significant depletion of P_d was visible concomitantly with an important P_d intake (1.0 of P_d mmol m^{-2} day^{-1}). We hypothesized that P_d intake results from biotic demand in sediment surface imposed by bacterial activity (Khoshmanesh et al., 2002) rather than from oxide–P_d interactions (no variation of P_{asc}/Fe_{asc} ratio was observed between spring and summer surveys; see Appendix 4). Porewater profiles in August (MD2) did not differ much from June (MD1 period), suggesting that diagenetic processes at the upstream part of the Loire estuary were close to steady state at depth, while diagenetic processes at the surface were delayed by progressive infilling of cracks.

According to our results, diagenetic and benthic fluxes are rhythmed by hydrological forces in the Loire estuary. Figure 8 summarizes benthic processes and exchanges through the 2020–2021 hydrological cycle.

4.4 Sediment and water column contributions to nutrient and oxygen stock

Respective water and sediment contributions to oxygen and nutrient uptake were estimated according to the available solute stock in the upstream part of the estuarine system and the water residence time (Figure 7). Confirming the importance of water column demand in highly turbid ecosystems, the water column reactivity constitutes the main oxygen uptake for the Loire

estuarine system during mid and low-discharge periods. Our estimation shows that water column reactivity was responsible for the consumption of 39% to 50% of the initial upstream stock of oxygen. Note that the simple model proposed does not take into account possible oxygen replenishment by atmospheric exchanges. Direct oxygen consumption by sediment represents up to 31% of the initial upstream oxygen stock during the low-discharge period. Despite the critical oxygen demand caused by methane bubbling during the flood, consequences on oxygen concentration in the water column were limited by a particularly short water residence time (0.9 day). These results corroborated several studies demonstrating the importance of sediment in the total oxygen demand in shallow aquatic systems (Sohma et al., 2008; Zhang et al., 2017).

Far from being the little brother of water column, sediment contribution to oxygen demand might be masked by the nature of water column and sediment interactions. Indeed, on two occasions during a hydrological year (HD and MD1 periods), sediment contributed to more than double the ΣNH_3 stock in the water column (e.g., 162% increase under sediment influence during the MD1 survey). Assuming complete nitrification of ammonium ($NH_4 +2O_2 \rightarrow NO_3^- + H_2O + 2H^+$; Liu and Wang, 2012), sediment ΣNH_3 efflux may have constituted 17% to 54% of the daily biogeochemical oxygen demand in water column (BOD) measured during summer 2021. However, previous studies demonstrated that nitrification is limited downstream the Loire estuary (Abril et al., 2003), highlighting the uncertainty in sediment contribution to summer hypoxia. On the other hand, ammonia constitutes an essential co-factor to nitrogen assimilation for photosynthetic species (Glibert et al., 2016) and a privileged form of nitrogen uptake for opportunistic species such as heterotrophic bacteria living in the Loire turbid estuary (Middelburg and Nieuwenhuize, 2000), which are responsible for a significant fraction of oxygen decrease in TMZ (Relexans et al., 1988).

Sediment contribution was particularly variable along the hydrological year according to the dissolved stock of P_d (Figure 6). During the hypoxic summer period, the sediment compartment controlled P_d efflux thanks to a persistent oxide production (by NO_3^- and oxides interaction). This control was shut down by the exceptional magnitude of the flood permitting the release of large P_d quantities by the sediment into the overlying water column (30% of increase under sediment influence). Control of P_d efflux was rapidly restored as evidenced by the absence of P_d efflux from sediment at the beginning of the oxic summer period (MD1) and the active intake during the MD2 survey (reducing by 75% P_d in water column). Our results demonstrate a significant role of sediment in the release of inherited phosphorus that contributes to the delay of the mitigation of eutrophication.

4.5 Perspectives and hypoxia management

Our results demonstrate the importance of the contribution of subtidal sediments to estuarine hypoxia. This study highlights the need to integrate the sediment compartment to define water policy management, using simplified modeling such as the residence time model. Nevertheless, in order to add sediment to biogeochemical models, several points of improvement are already emerging from our results. The first one is the incorporation of non-diffusive fluxes and
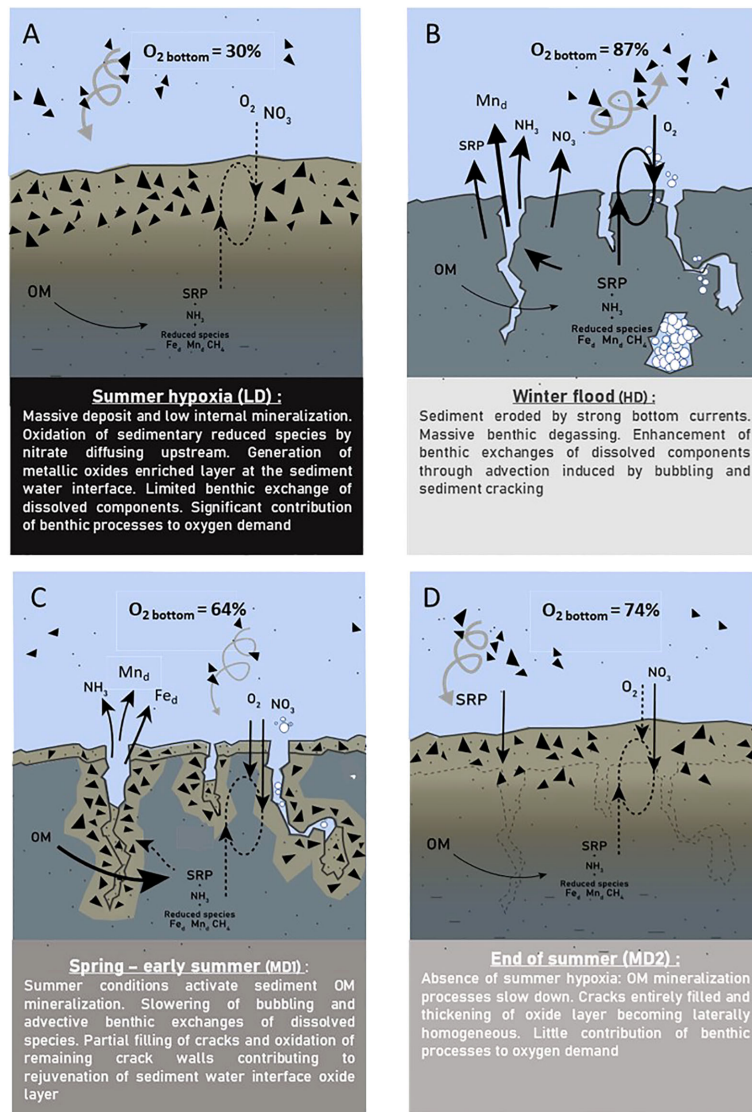
FIGURE 8
Conceptual functioning of benthic processes at Le Pellerin for 2020−2021 in the context of hydrological contrasted conditions. **(A)** August 2020.
(B) February 2021. **(C)** June 2021. **(D)** August 2021. Dark triangles indicate metallic oxides and hydroxides. Black arrows indicate dissolved exchanges.
Brown spirals specify SPM sedimentation/resuspension.

hydro-sedimentary processes to apprehend the high annual variability of the water–sediment exchanges. Indeed, during major floods, erosion processes can lead to the release of methane trapped in the estuarine sediments, enhancing the active transport of solute species at the sediment–water interface (O'Hara et al., 1995). This release may also occur during summer dredging operations undertaken to maintain harbor activity and upper estuarine traffic. On the contrary, during low fluvial discharge conditions, which promote the presence of TMZ in the upper estuary, massive sediment deposition limits water advection throughout the sediment. This induces a significant reduction of water–sediment exchange, which becomes mainly diffusive in agreement with conventional early diagenetic models. Understanding advective benthic transfer is important, because permeable sediments are

particularly sensitive to advective porewater transport (Santos et al., 2012) and represent an important part of the estuarine habitat.

A second way to improve this model is the inclusion of intertidal sediments and the immersion–emersion dynamics imposed by the tidal cycles within the estuary. A comparison with the intertidal dynamics previously explored by Thibault de Chanvalon et al. (2016) demonstrated clear differences in subtidal functioning. The occurrence of bioturbation, different erosion/deposition dynamics, and the temporary submersion of sediment illustrate the wide gap between intertidal and subtidal sediment systems. As an example of differentiated functioning, iron and manganese cycles demonstrated a complete asynchrony during supply and remobilization events. Capturing the connectivity between the two compartments is of vital importance to achieve a complete scheme of sediment contribution to water column hypoxia.

5 Conclusion

Our study confirms the role of the sediment compartment in hypoxic phenomena. Directly or indirectly, the sediment compartment actively contributes to oxygen consumption and eutrophication during the summer low-discharge period, confirming our preliminary hypothesis. However, the role of sediment appears to be much more complex on the nutrient budget than often described in the literature. Despite exposure to hypoxic conditions, the benthic compartment maintains its barrier of metal oxides and therefore strongly controls P_d bioavailability in the water column. The interaction between metal oxides and nitrate appeared to be the last line of defense to limit P_d escape and the aggravation of hypoxia. Furthermore, our study highlights the importance of extreme floods on benthic oxygen demand and nutrient benthic recycling that can be enhanced by several orders of magnitude due to intense erosion of fluvial bed and its subsequent gas ebullition. Despite evident logistic limitations, such events need to be better studied in order to be considered by the scientific community in their predictive modeling. Therefore, our study raises the importance for modelers and managers, despite their efforts, to take into account the complexity of benthic processes to better predict the evolution of biogeochemical functioning of macrotidal estuaries, especially during droughts and floods, extreme conditions that tend to be more frequent for temperate latitudes.

Data availability statement

The original contributions presented in the study are included in the article/Supplementary Material. Further inquiries can be directed to the corresponding authors.

Author contributions

Funding

Acknowledgments

Conflict of interest

The authors declare that the research was conducted in the absence of any commercial or financial relationships that could be construed as a potential conflict of interest.

Publisher's note

All claims expressed in this article are solely those of the authors and do not necessarily represent those of their affiliated organizations, or those of the publisher, the editors and the reviewers. Any product that may be evaluated in this article, or claim that may be made by its manufacturer, is not guaranteed or endorsed by the publisher.

Supplementary material

The Supplementary Material for this article can be found online at: https://www.frontiersin.org/articles/10.3389/fmars.2023.1083377/full#supplementary-material

References

Abril, G., Commarieu, M.-V., Sottolichio, A., Bretel, P., and Guérin, F. (2009). Turbidity limits gas exchange in a large macrotidal estuary. *Estuarine Coast. Shelf Sci.* 83, 342–348. doi: 10.1016/j.ecss.2009.03.006

Abril, G., Etcheber, H., Delille, B., Frankignoulle, M., and Borges, A. V. (2003). Carbonate dissolution in the turbid and eutrophic Loire estuary. *Mar. Ecol. Prog. Ser.* 259, 129–138. doi: 10.3354/meps259129

Algar, C. K., Boudreau, B. P., and Barry, M. A. (2011a). Release of multiple bubbles from cohesive sediments. *Geophysical Res. Lett.* 38. doi: 10.1029/2011GL046870

Algar, C. K., Boudreau, B. P., and Barry, M. A. (2011b). Initial rise of bubbles in cohesive sediments by a process of viscoelastic fracture. *J. Geophysical Research: Solid Earth* 116. doi: 10.1029/2010JB008133

Aminot, A., Kérouel, R., and Coverly, S. C. (2009). "Nutrients in seawater using segmented flow analysis," in *Practical guidelines for the analysis of seawater* (CRC press), 155–190. doi: 10.1201/9781420073072.ch8

Anschutz, P., Zhong, S., Sundby, B., Mucci, A., and Gobeil, C. (1998). Burial efficiency of phosphorus and the geochemistry of iron in continental margin sediments. *Limnology Oceanography* 43, 53–64. doi: 10.4319/lo.1998.43.1.0053

Bendschneider, K., and Robinson, R. J. (1952). *A new spectrophotometric method for the determination of nitrite in sea water. Journal of Marine Research* 11 (1952), 87–96.

Berner, R. A. (1980). *Early diagenesis: A theoretical approach* (Princeton University Press). doi: 10.2307/j.ctvx8b6p2

Blanchet-Letrouvé, I., Lafont, A.-G., Poirier, L., Baloche, S., Zalouk-Vergnoux, A., Dufour, S., et al. (2013). Vg mRNA induction in an endangered fish species (Anguilla anguilla) from the Loire estuary (France). *Ecotoxicology Environ. Saf.* 97, 103–113. doi: 10.1016/j.ecoenv.2013.07.019

Borges, A. V., and Abril, G. (2011). "Carbon dioxide and methane dynamics in estuaries," in *Treatise on estuarine and coastal science*. Eds. E. Wolanski and D. McLusky (Waltham: Academic Press), 119–161. doi: 10.1016/B978-0-12-374711-2.00504-0

Bowman, G. T., and Delfino, J. J. (1980). Sediment oxygen demand techniques: A review and comparison of laboratory and *in situ* systems. *Water Res.* 14, 491–499. doi: 10.1016/0043-1354(80)90215-8

Burdige, D. J. (1993). The biogeochemistry of manganese and iron reduction in marine sediments. *Earth-Science Rev.* 35, 249–284. doi: 10.1016/0012-8252(93)90040-E

Burdige, D. J. (2006). *Geochemistry of marine sediments* (Princeton University Press). doi: 10.2307/j.ctv131bw7s

Burdige, D. J., and Zheng, S. (1998). The biogeochemical cycling of dissolved organic nitrogen in estuarine sediments. *Limnology Oceanography* 43, 1796–1813. doi: 10.4319/lo.1998.43.8.1796

Burgin, A. J., Yang, W. H., Hamilton, S. K., and Silver, W. L. (2011). Beyond carbon and nitrogen: How the microbial energy economy couples elemental cycles in diverse ecosystems. *Front. Ecol. Environ.* 9, 44–52. doi: 10.1890/090227

Canfield, D. E. (1989). Sulfate reduction and oxic respiration in marine sediments: Implications for organic carbon preservation in euxinic environments. *Deep Sea Res. Part A. Oceanographic Res. Papers* 36, 121–138. doi: 10.1016/0198-0149(89)90022-8

Carey, C. C., and Rydin, E. (2011). Lake trophic status can be determined by the depth distribution of sediment phosphorus. *Limnology and oceanography* 56(6), 2051–2063.

Center, E. (2005). "Estuarine respiration: An overview of benthic, pelagic, and whole system respiration," in *Respiration in aquatic ecosystems*, 122.

Centre national pour l'exploitation des océans (1984) *Rapport du comité scientifique de l'estuaire de la Loire (Rapport scientifique et techniques no. 55).*

Cheng, C. H., Huettel, M., and Wildman, R. A. (2014). Ebullition-enhanced solute transport in coarse-grained sediments. *Limnology Oceanography* 59, 1733–1748. doi: 10.4319/lo.2014.59.5.1733

Cheviet, C., Violeau, D., and Guesmia, M. (2002). "Numerical simulation of cohesive sediment transport in the Loire estuary with a three-dimensional model including new parameterisations," in *Proceedings in marine science* (Elsevier), 529–543. doi: 10.1016/S1568-2692(02)80038-9

Coynel, A., Gorse, L., Curti, C., Schafer, J., Grosbois, C., Morelli, G., et al. (2016). Spatial distribution of trace elements in the surface sediments of a major European estuary (Loire estuary, france): Source identification and evaluation of anthropogenic contribution. *J. Sea Research Recent past sedimentary biogeochemical benthic ecosystem Evol. Loire Estuary (Western France)* 118, 77–91. doi: 10.1016/j.seares.2016.08.005

Dai, M., Wang, L., Guo, X., Zhai, W., Li, Q., He, B., et al. (2008). Nitrification and inorganic nitrogen distribution in a large perturbed river/estuarine system: The pearl river estuary, China. *Biogeosciences* 5, 1227–1244. doi: 10.5194/bg-5-1227-2008

De Blois, C. J., and Wind, H. G. (1995). Assessment of flood damages and benefits of remedial actions: "What are the weak links?"; with application to the Loire. *Phys. Chem. Earth* 20, 491–495. doi: 10.1016/S0079-1946(96)00011-0

Dhivert, E., Grosbois, C., Rodrigues, S., and Desmet, M. (2015). Influence of fluvial environments on sediment archiving processes and temporal pollutant dynamics (Upper Loire river, France). *Sci. total Environ.* 505, 121–136. doi: 10.1016/j.scitotenv.2014.09.082

Etcheber, H., Taillez, A., Abril, G., Garnier, J., Servais, P., Moatar, F., et al. (2007). Particulate organic carbon in the estuarine turbidity maxima of the gironde, Loire and seine estuaries: Origin and lability. *Hydrobiologia* 588, 245–259. doi: 10.1007/s10750-007-0667-9

Fick, A. (1855). V. On liquid diffusion. *Philosophical Magazine* 410, 30–39. doi: 10.1080/14786445508641925

Flury, S., Glud, R. N., Premke, K., and McGinnis, D. F. (2015). Effect of sediment gas voids and ebullition on benthic solute exchange. *Environ. Sci. Technol.* 49, 10413–10420. doi: 10.1021/acs.est.5b01967

Ghaisas, N. A., Maiti, K., and White, J. R. (2019). Coupled iron and phosphorus release from seasonally hypoxic Louisiana shelf sediment. *Estuarine Coast. Shelf Sci.* 219, 81–89. doi: 10.1016/j.ecss.2019.01.019

Glibert, P. M., Wilkerson, F. P., Dugdale, R. C., Raven, J. A., Dupont, C. L., Leavitt, P. R., et al. (2016). Pluses and minuses of ammonium and nitrate uptake and assimilation by phytoplankton and implications for productivity and community composition, with emphasis on nitrogen-enriched conditions. *Limnology Oceanography* 61, 165–197. doi: 10.1002/lno.10203

Gran, G. (1952). Determination of the equivalence point in potentiometric titrations. part II. *Analyst* 77, 661–671. doi: 10.1039/an9527700661

Guillaud, J.-F., Aminot, A., Delmas, D., Gohin, F., Lunven, M., Labry, C., et al. (2008). Seasonal variation of riverine nutrient inputs in the northern bay of Biscay (France), and patterns of marine phytoplankton response. *J. Mar. Systems Oceanography Bay Biscay* 72, 309–319. doi: 10.1016/j.jmarsys.2007.03.010

Hansen, J., Reitzel, K., Jensen, H. S., and Andersen, F.Ø. (2003). Effects of aluminum, iron, oxygen and nitrate additions on phosphorus release from the sediment of a Danish softwater lake. *Hydrobiologia* 492, 139–149. doi: 10.1023/A:1024826131327

Hayami, Y., Wada, M., Umezawa, Y., Fujii, N., Nakamura, A., and Mori, F. (2019). Hypoxic water mass in the highly turbid well-mixed macrotidal rokkaku river estuary, ariake Sea, Japan. *Estuarine Coast. Shelf Sci.* 219, 210–222. doi: 10.1016/j.ecss.2019.02.011

Huang, F., Lin, X., and Yin, K. (2022). Effects of algal-derived organic matter on sediment nitrogen mineralization and immobilization in a eutrophic estuary. *Ecol. Indic.* 138, 108813. doi: 10.1016/j.ecolind.2022.108813

Hupfer, M., and Lewandowski, J. (2008). Oxygen controls the phosphorus release from Lake Sediments–a long-lasting paradigm in limnology. *International Review of Hydrobiology* 93(4-5), 415–32.

Hydro, B. (2021). *Banque nationale de donnée pour l'hydrométrie et l'hydrologie. banque hydro, ministère de l'Environnement et du développement durable* (Paris). Available at: http://www.hydro.eaufrance.fr/accueil

Jalón-Rojas, I., Schmidt, S., Sottolichio, A., and Bertier, C. (2016). Tracking the turbidity maximum zone in the Loire estuary (France) based on a long-term, high-resolution and high-frequency monitoring network. *Continental Shelf Res.* 117, 1–11. doi: 10.1016/j.csr.2016.01.017

Jamieson, J., Prommer, H., Kaksonen, A. H., Sun, J., Siade, A. J., Yusov, A., et al. (2018). Identifying and quantifying the intermediate processes during nitrate-dependent Iron(II) oxidation. *Environ. Sci. Technol.* 52, 5771–5781. doi: 10.1021/acs.est.8b01122

Janssen, F., Huettel, M., and Witte, U. (2005). Pore-water advection and solute fluxes in permeable marine sediments (II): Benthic respiration at three sandy sites with different permeabilities (German bight, north Sea). *Limnology Oceanography* 50, 779–792. doi: 10.4319/lo.2005.50.3.0779

Khoshmanesh, A., Hart, B. T., Duncan, A., and Beckett, R. (2002). Luxury uptake of phosphorus by sediment bacteria. *Water Res.* 36, 774–778. doi: 10.1016/S0043-1354(01)00272-X

Kristiansen, K. D., Kristensen, E., and Jensen, E. M. H. (2002). The influence of water column hypoxia on the behaviour of manganese and iron in sandy coastal marine sediment. *Estuarine Coast. Shelf Sci.* 55, 645–654. doi: 10.1006/ecss.2001.0934

Lajaunie-Salla, K., Wild-Allen, K., Sottolichio, A., Thouvenin, B., Litrico, X., and Abril, G. (2017). Impact of urban effluents on summer hypoxia in the highly turbid gironde estuary, applying a 3D model coupling hydrodynamics, sediment transport and biogeochemical processes. *J. Mar. Syst.* 174, 89–105. doi: 10.1016/j.jmarsys.2017.05.009

Lajaunie-Salla, K., Sottolichio, A., Schmidt, S., Litrico, X., Binet, G., and Abril, G. (2018). Future intensification of summer hypoxia in the tidal Garonne River (SW France) simulated by a coupled hydro sedimentary-biogeochemical model. *Environmental Science and Pollution Research* 25(32), 31957–31970.

Lanoux, A., Etcheber, H., Schmidt, S., Sottolichio, A., Chabaud, G., Richard, M., et al. (2013). Factors contributing to hypoxia in a highly turbid, macrotidal estuary (the gironde, France). *Environ. Sci.: Processes Impacts* 15, 585–595. doi: 10.1039/C2EM30874F

Lenstra, W. K., Hermans, M., Séguret, M. J. M., Witbaard, R., Severmann, S., Behrends, T., et al. (2021). Coastal hypoxia and eutrophication as key controls on benthic release and water column dynamics of iron and manganese. *Limnology Oceanography* 66, 807–826. doi: 10.1002/lno.11644

Liu, G., and Wang, J. (2012). Probing the stoichiometry of the nitrification process using the respirometric approach. *Water Res.* 46, 5954–5962. doi: 10.1016/j.watres.2012.08.006

Lorrain, A., Savoye, N., Chauvaud, L., Paulet, Y.-M., and Naulet, N. (2003). Decarbonation and preservation method for the analysis of organic c and n contents and stable isotope ratios of low-carbonated suspended particulate material. *Analytica Chimica Acta* 491, 125–133. doi: 10.1016/S0003-2670(03)00815-8

Luther, G. W., Sundby, B., Lewis, B. L., Brendel, P. J., and Silverberg, N. (1997). Interactions of manganese with the nitrogen cycle: Alternative pathways to dinitrogen. *Geochimica Cosmochimica Acta* 61, 4043–4052. doi: 10.1016/S0016-7037(97)00239-1

Marchand, J. (1993). The influence of seasonal salinity and turbidity maximum variations on the nursery function of the Loire estuary (France). *Netherland J. Aquat. Ecol.* 27, 427–436. doi: 10.1007/BF02334804

Metzger, E., Barbe, A., Cesbron, F., de Chanvalon, A. T., Jauffrais, T., Jézéquel, D., et al. (2019). Two-dimensional ammonium distribution in sediment pore waters using a new colorimetric diffusive equilibration in thin-film technique. *Water Res. X* 2, 100023. doi: 10.1016/j.wroa.2018.100023

Metzger, E., and Maillet, G. M. (2021). *REBELRED cruises, RV thalia and RV côtes de la manche.* doi: 10.17600/18001620

Metzger, E., Simonucci, C., Viollier, E., Sarazin, G., Prévot, F., and Jézéquel, D. (2007). Benthic response to shellfish farming in thau lagoon: Pore water signature. *Estuarine Coast. Shelf Sci.* 72, 406–419. doi: 10.1016/j.ecss.2006.11.011

Middelburg, J., and Nieuwenhuize, J. (2000). Uptake of dissolved inorganic nitrogen in turbid, tidal estuaries. *Mar. Ecol. Prog. Ser.* 192, 79–88. doi: 10.3354/meps192079

Middelburg, J. J., Nieuwenhuize, J., Iversen, N., Høgh, N., De Wilde, H., Helder, W., et al. (2002). Methane distribution in European tidal estuaries. *Biogeochemistry* 59, 95–119. doi: 10.1023/A:1015515130419

Moncelon, R., Gouazé, M., Pineau, P., Bénéteau, E., Bréret, M., Philippine, O., et al. (2021). Coupling between sediment biogeochemistry and phytoplankton development in a temperate freshwater marsh (Charente-maritime, france): Evidence of temporal pattern. *Water Res.* 189, 116567. doi: 10.1016/j.watres.2020.116567

Moncelon, R., Metzger, E., Pineau, P., Emery, C., Bénéteau, E., de Lignières, C., et al. (2022). Drivers for primary producers' dynamics: New insights on annual benthos pelagos monitoring in anthropised freshwater marshes (Charente-maritime, France). *Water Res.* 221, 118718. doi: 10.1016/j.watres.2022.118718

Nichols, F. H., Cloern, J. E., Luoma, S. N., and Peterson, D. H. (1986). The modification of an estuary. *Science* 231, 567–573. doi: 10.1126/science.231.4738.567

O'Hara, S. C. M., Dando, P. R., Schuster, U., Bennis, A., Boyle, J. D., Chui, F. T. W., et al. (1995). Gas seep induced interstitial water circulation: Observations and environmental implications. *Continental Shelf Res.* 15, 931–948. doi: 10.1016/0278-4343(95)80003-V

Oviatt, C., Smith, L., Krumholz, J., Coupland, C., Stoffel, H., Keller, A., et al. (2017). Managed nutrient reduction impacts on nutrient concentrations, water clarity, primary production, and hypoxia in a north temperate estuary. *Estuarine Coast. Shelf Sci.* 199, 25–34. doi: 10.1016/j.ecss.2017.09.026

Owings, S. M., Luther, G. W., and Taillefert, M. (2019). Development of a rate law for arsenite oxidation by manganese oxides. *Geochimica Cosmochimica Acta* 250, 251–267. doi: 10.1016/j.gca.2019.02.003

Pastor, L., Deflandre, B., Viollier, E., Cathalot, C., Metzger, E., Rabouille, C., et al. (2011). Influence of the organic matter composition on benthic oxygen demand in the rhône river prodelta (NW Mediterranean Sea). *Continental Shelf Res.* 31, 1008–1019. doi: 10.1016/j.csr.2011.03.007

Ratmaya, W., Soudant, D., Salmon-Monviola, J., Plus, M., Cochennec-Laureau, N., Goubert, E., et al. (2019). Reduced phosphorus loads from the Loire and vilaine rivers were accompanied by increasing eutrophication in the vilaine bay (south Brittany, France). *Biogeosciences* 16, 1361–1380. doi: 10.5194/bg-16-1361-2019

R Core Team (2013). *R: A language and environment for statistical computing*.

Relexans, J. C., Meybeck, M., Billen, G., Brugeaille, M., Etcheber, H., and Somville, M. (1988). Algal and microbial processes involved in particulate organic matter dynamics in the Loire estuary. *Estuarine Coast. Shelf Sci.* 27, 625–644. doi: 10.1016/0272-7714(88)90072-8

Ross, M. A., and Mehta, A. J. (1989). On the mechanics of lutoclines and fluid mud. *J. Coast. Res.*, 51–62.

Sanchez, M., and Levacher, D. (2008). Erosion d'une vase de l'estuaire de la Loire sous l'action du courant. *Bull. Eng. Geol Environ.* 67, 597–605. doi: 10.1007/s10064-008-0159-9

Santos, I. R., Eyre, B. D., and Huettel, M. (2012). The driving forces of porewater and groundwater flow in permeable coastal sediments: A review. *Estuarine Coast. Shelf Sci.* 98, 1–15. doi: 10.1016/j.ecss.2011.10.024

Sarazin, G., Michard, G., and Prevot, F. (1999). A rapid and accurate spectroscopic method for alkalinity measurements in sea water samples. *Water Res.* 33, 290–294. doi: 10.1016/S0043-1354(98)00168-7

Schmidt, S., de Stigter, H. C., and van Weering, T. C. E. (2001). Enhanced short-term sediment deposition within the nazaré canyon, north-East Atlantic. *Mar. Geology* 173(1-4), 55–67. doi: 10.1016/S0025-3227(00)00163-8

Schmidt, S., Diallo, I. I., Derriennic, H., Fallou, H., and Lepage, M. (2019). Exploring the susceptibility of turbid estuaries to hypoxia as a prerequisite to designing a pertinent monitoring strategy of dissolved oxygen. *Front. Mar. Sci.* 6. doi: 10.3389/fmars.2019.00352

Schnetger, B., and Lehners, C. (2014). Determination of nitrate plus nitrite in small volume marine water samples using vanadium (III) chloride as a reduction agent. *Mar. Chem.* 160, 91–98. doi: 10.1016/j.marchem.2014.01.010

Soetaert, K., Hofmann, A. F., Middelburg, J. J., Meysman, F. J., and Greenwood, J. (2007). Reprint of "The effect of biogeochemical processes on pH". *Marine Chemistry* 106 (1-2), 380–401.

Sohma, A., Sekiguchi, Y., Kuwae, T., and Nakamura, Y. (2008). A benthic-pelagic coupled ecosystem model to estimate the hypoxic estuary including tidal flat - Model description and validation of seasonal/daily dynamics. Ecol. Model 215, 10–39.

Steinbach, P. (2001). Effets cumulés sur les poissons migrateurs, état et restauration des grands axes de migration du bassin de la Loire. *Hydroêcol. Appl.* 13, 115–130. doi: 10.1051/hydro:2001011

Talke, S. A., de Swart, H. E., and De Jonge, V. N. (2009). An idealized model and systematic process study of oxygen depletion in highly turbid estuaries. *Estuaries coasts* 32, 602–620. doi: 10.1007/s12237-009-9171-y

Thibault de Chanvalon, A., Mouret, A., Knoery, J., Geslin, E., Péron, O., and Metzger, E. (2016). Manganese, iron and phosphorus cycling in an estuarine mudflat, Loire, France. *J. Sea Research Recent past sedimentary biogeochemical benthic ecosystem Evol. Loire Estuary (Western France)* 118, 92–102. doi: 10.1016/j.seares.2016.10.004

Whitney, M. M., and Vlahos, P. (2021). Reducing hypoxia in an urban estuary despite climate warming. *Environ. Sci. Technol.* 55, 941–951. doi: 10.1021/acs.est.0c03964

Yang, H., Yu, S., and Lu, H. (2021). Iron-coupled anaerobic oxidation of methane in marine sediments: A review. *J. Mar. Sci. Eng.* 9, 875. doi: 10.3390/jmse9080875

Yu, L., and Gan, J. (2021). Mitigation of eutrophication and hypoxia through oyster aquaculture: An ecosystem model evaluation off the pearl river estuary. *Environ. Sci. Technol.* 55, 5506–5514. doi: 10.1021/acs.est.0c06616

Zhang, H., Zhao, L., Sun, Y., Wang, J., and Wei, H. (2017). Contribution of sediment oxygen demand to hypoxia development off the changjiang estuary. *Estuarine Coast. Shelf Sci.* 192, 149–157. doi: 10.1016/j.ecss.2017.05.006